Journal of Building Engineering 75 (2023) 107026

Contents lists available at ScienceDirect

Journal of Building Engineering

journal homepage: www.elsevier.com/locate/jobe

The potential usage of waste ferrochrome slag in alkali-activated mixes

Nausad Miyan [a], Tarik Omur [b], Nihat Kabay [b,*], Burak Birol [c]

[a] LBA Design and Consultancy, 34750, Istanbul, Turkiye
[b] Yildiz Technical University, Department of Civil Engineering, 34220, Istanbul, Turkiye
[c] Yildiz Technical University, Department of Metallurgical and Materials Engineering, 34210, Istanbul, Turkiye

ARTICLE INFO

Keywords:
Ferrochrome slag
Blast furnace slag
Alkali-activation
Rheology
pH evolution

ABSTRACT

Ferrochrome slag (FCS) is a by-product of the stainless-steel industry which is mostly discarded in landfills without being efficiently utilized. The production of industrial solid wastes like FCS has been increasing for several decades and escalating the environmental risks associated with them. To address this issue, this study concentrated on the usage of FCS as a partial substitution for blast furnace slag (BS) in manufacturing alkali-activated paste and mortar. BS was replaced with FCS in varying proportions up to 30% (wt.%) and activated with varying Na_2O dosages. The fresh, physical, mechanical, and microstructural properties were investigated. The test outcomes indicated that FCS incorporation was beneficial in improving the flowability by consistently reducing both yield stress and plastic viscosity more than 54% and 70%, respectively, when FCS replacement was 30%. Furthermore, the inclusion of FCS alleviated the rapid setting issue of BS-based alkali-activated systems by delaying the setting times. The increase in Na_2O concentration remarkably decreased the water absorption, open porosity and capillary sorptivity of the mortars, while no adverse effect was observed on the physical properties of the mortars with the FCS addition. The compressive strength of mortars increased between 152% and 254% when Na_2O dosage was increased from 4% to 8%, while strength was mostly preserved with the addition of FCS. The higher Si/Al atomic ratio and the higher pH values was found favorable for the higher compressive strength of the mixes. The primary reaction product was found as C-A-S-H gels, whereas FCS addition increased the crystalline phases and favored the formation of M-A-S-H gels.

1. Introduction

The tremendous growth of the world population, the technological and industrial development, and the increase in consumption of natural resources have led to a rapid increase in industrial wastes and by-products [1]. Industrial waste products occupy precious land mass, pollute the environment, and pose significant disposal issues. The most effective strategy for managing solid waste is the "5Rs" approach that is reduction, recovery, recycling, reuse, and research [2]. Several studies have been carried out to identify all viable reuse and recycling techniques in response to increasing demand of natural resources to minimize waste and pollution [3–5]. Additionally, the construction industry, which is expanding at an alarming rate, is one of the largest waste producers and consumers of natural resources. This increases the concerns regarding waste disposal and the consumption of natural resources, which causes substantial threat to environmental equilibrium. One promising approach to overcome environmental and economic issues is

* Corresponding author. Yildiz Technical University, Department of Civil Engineering, Construction Materials Division, 34220, Istanbul, Turkiye.
E-mail address: nkabay@yildiz.edu.tr (N. Kabay).

https://doi.org/10.1016/j.jobe.2023.107026
Received 22 March 2023; Received in revised form 9 May 2023; Accepted 5 June 2023
Available online 6 June 2023
2352-7102/© 2023 Elsevier Ltd. All rights reserved.

industrial symbiosis, where the waste products of one industry may become the raw materials for another [6,7]. By harnessing the benefits of this circular and collaborative approach, waste disposal can be reduced, resources can be conserved, and a more sustainable future can be promoted. For instance, the construction sector is an excellent opportunity to implement the 5Rs approach due to the abundant use of concrete, which allows the use of waste materials. Even in the production of aggregate, which is one of the components of concrete, many waste materials such as marble powder and municipal solid waste incineration fly ash have been integrated with the pelletization process and have contributed to the sustainability of the construction sector [8,9].

Ferrochrome slag (FCS) is a waste obtained during the manufacturing of ferrochrome. In electric arc furnaces, the oxide of chromium ore is combined with coke as a reduction agent at a temperature between 1500 °C and 1700 °C to generate ferrochrome metal. FCS is generated after the gravity separation from the metal and allowed to cool in the air progressively [2]. For each ton of ferrochrome production, 1.1–1.6 tonnes of FCS waste is generated, and the annual worldwide production of FCS is estimated to be approximately 12–16 million metric tons [10,11]. Furthermore, the annual global production of FCS is estimated to increase at the rate of approximately 3–5% [12]. However, a small portion of manufactured FCS is utilized for construction purposes, while the remainder is disposed [13]. The massive accumulation of this waste material necessitates huge landfill areas, which is economically unfavorable and when deposited to open atmosphere creates environmental issues such as leaching of heavy metals and groundwater contamination, biodegradation, and air pollution [1]. Therefore, it is vital to evaluate FCS solid waste for viable applications and its utilization in alkali-activated materials (AAMs) can be an alternate method considering the fact that FCS is rich in alumina and silica.

Another reason for the consideration of FCS in AAM systems instead of cementitious systems, is its high MgO content. The presence of MgO in high concentrations can delay the cement hydration and prolong its setting time [14], as well as cause substantial volume expansion in cementitious materials [15]. Therefore, the utilization of FCS in an alkali-activated system is an opportunity to manage the disposal of this solid waste and offer an alternative binder.

AAMs are construction materials produced by mixing an alkaline solution with a reactive powder, such as fly ash, rice husk ash, silica fume, metakaolin, blast furnace slag (BS), volcanic ash, rice husk ash, and volcanic tuff [16–20]. The resulting material dominates similar or better properties compared to conventional cementitious materials. AAMs are also comparatively more environmentally friendly and have lower carbon footprint [21,22]. In addition, the alkali-activated system has the ability to immobilize the potential heavy and hazardous elements found in the waste materials [23,24]. FCS typically consists of silicon, aluminum, iron, calcium, magnesium, and chromium. The exact composition of FCS can vary depending on the production process and the source of the raw materials. Considering the oxide compositions of FCS, chromium is one of the primary pollutants due to its potential leaching. Erdem et al. [25], examined the chromium leaching behavior of crushed and ground FCS obtained from Elazig region (Turkiye) with the toxicity characteristic leaching procedure (TCLP) and found that the chromium leaching of FCS was lower than the limit value (5 mg/l for Cr) specified in the US Environmental Protection Agency (US EPA). Furthermore, it has been reported that the amount and type of chromium (Cr^{+3} or Cr^{+6}) present in FCS may affect its leaching behavior, especially in long periods [26].

As a potential construction material, FCS may have advantages and disadvantages. The utilization of FCS as a precursor can not only save landfills but also prevent leaching issues. On the other hand, the low CaO content of FCS may restrict its use in alkali-activated systems as a sole binder or at high ratios by affecting the hardening process under ambient conditions. Moreover, additional transportation costs may arise as the areas where FCS is produced or stored are often far from construction sites or concrete production facilities. However, the higher specific gravity of FCS compared to other metallurgical slags like BS can alleviate this disadvantage. The high specific gravity of powders (potential precursors) can help lower their production and delivery costs. For instance, more material can be produced by employing the same amount of powder in a smaller volume, reducing production and transportation expenses.

FCS has been previously employed as coarse and fine aggregates in concrete or mortar [12,27–31] or road constructions due to its dense structure [32]. Gencel et al. [30] studied the characteristics of concrete incorporating FCS as a coarse aggregate and found promising results in terms of tensile strength and abrasion resistance. Panda et al. [29] indicated that replacing the natural sand with FCS fine aggregate yielded similar compressive strength without leaching of heavy metals like chromium. However, Dash and Patro [31] found that the compressive strength of concrete slightly decreased with an increase in the FCS fine aggregate content.

The utilization of FCS in AAMs have also been reported in the literature. Nath [13] studied the geopolymerization of FCS and fly ash blend and reported that the low reactivity of fly ash-based geopolymers at ambient conditions could be improved with the incorporation of FCS powder which result in increased strength. The geopolymerization of 100% FCS powder activated with various dosages of sodium hydroxide (NaOH) and sodium silicate (Na_2SiO_3) solution was reported by Ref. [33], where the sole usage of FCS as a precursor in AAM yielded about 22 MPa compressive strength at 28 days without heat curing. Özcan and Karakoç [34] investigated the acid resistance of FCS and BS-based geopolymer concrete and found that incorporation of FCS enhanced the acid resistance of BS-based geopolymers and reduced surface deterioration after acid exposure.

The use of FCS in alkali-activated mixtures can reduce costs and provide economic benefits for construction companies. Since FCS is a waste material, it can often be cheaper than traditional raw materials, such as cement, silica fume, or rice husk ash, which requires various additional processes to obtain the final product. Additionally, the utilization of FCS powder in alkali-activated mortar or concrete can help reduce the industry's environmental impact by reducing the amount of waste sent to landfills and using less traditional raw materials. Furthermore, considering the annual availability of aluminosilicate binders in alkali-activated systems, the available amount of common precursors such as red mud, BS, and fly ash was respectively reported as 80, 390, and 800 million tonnes, significantly lower than the availability of cement (4000 million tonnes) [35]. Hence, the alkali-activated systems require the utilization of new aluminosilicate sources like FCS to compete and replace traditional cementitious systems.

The utilization of FCS powder as a sole binder and as a replacement material in fly ash or BS-based geopolymers have generally focused on the parameters such as setting time, mechanical properties, and acid and sulfate resistance. This study seeks to explore the

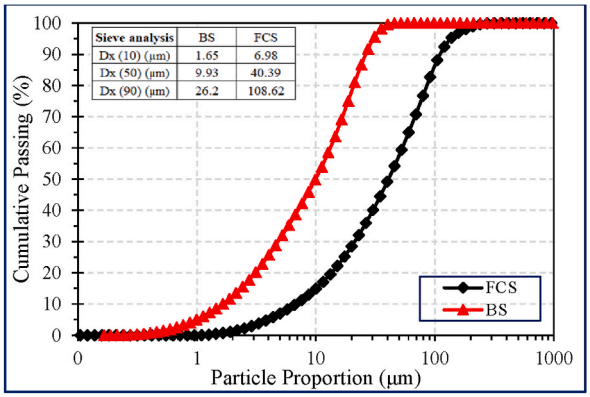


Fig. 1. Sieve size analysis results of FCS and BS.

effects of FCS addition and Na_2O dosage on the fresh, physical, mechanical, and microstructural properties of FCS and BS-based alkali-activated mortars and brings an insight on the factors affecting the strength deveopment by establishing correlations between compressive strength and pH value, and Si/Al ratio. For this purpose, alkali-activated pastes and mortars were manufactured by partially replacing BS with FCS and activated with two different Na_2O dosages (4% and 8%). The setting time, rheology, pH evolution, X-ray diffraction (XRD), and Scanning electron microscopy (SEM) analysis of paste samples and compressive strength, capillary sorptivity, water absorption, and open porosity of mortar samples were studied.

2. Materials and experimental procedures

2.1. Raw materials

FCS was collected from a ferrochrome production facility (Eti Krom Inc.), located in Elazığ, Turkey, which manufactures high carbon ferrochrome, whereas BS was locally sourced from the market. The particle size of FCS was reduced by a laboratory type disc grinder to enhance its reactivity. The particle size distribution (PSD) of FCS and BS are shown in Fig. 1, which indicates that the FCS is coarser than BS and the median particle size of BS and FCS were found as 9.93 μm and 40.39 μm, respectively. Furthermore, a wider range of PSD was observed in FCS particles compared to BS particles as FCS ranged approximately between 2 and 200 μm, whereas BS ranged between 0.4 and 40 μm. The chemical oxide components of BS and FCS based on the X-ray fluorescence (XRF) analysis are tabulated in Table 1. The sum of the SiO_2 and Al_2O_3 content exceeded 50% for both precursors, and the SiO_2/Al_2O_3 ratio of BS and FCS was obtained as 3.12 and 1.67, respectively. In addition, FCS was rich in MgO content (34.85%), while BS contained high amount of CaO (37.50%). The crystalline structure of the raw materials based on the XRD analysis is illustrated in Fig. 2. BS exhibited amorphous structure with a broad hump between 20° (2Θ) and 40° (2Θ), whereas several crystalline phases such as quartz (SiO_2) (#PDF 01-079-1915), forsterite (Mg_2SiO_4) (#PDF 00-021-1260), olivine ($(Mg, Fe)_2SiO_4$) (#PDF 96-900-6399), and spinel ($Mg(AlO_2)_2$) (#PDF 96-900-7117) were detected in FCS. The shape and surface morphology of BS and FCS particles are examined with SEM analysis and presented in Fig. 3. The irregular particle shapes without significant cellulosic/porous structures were observed in both FCS and BS particles. The alkaline activators were prepared using the readily available NaOH pellets (>99% purity) and liquid Na_2SiO_3 solution containing Na_2O and SiO_2, of 8.4% and 27.8%, respectively. The standard siliceous sand complying EN 196–1 was used as fine aggregate to manufacture the mortar samples.

2.2. Mixture proportions and specimen preparation

The mix design parameters of the alkali-activated mixes are presented in Table 2. The alkali-activated paste and mortar mixes contained 0, 10, 20, and 30% of FCS by mass of total binder. The combination of NaOH and Na_2SiO_3 solution with a constant M_s ratio (SiO_2/Na_2O) of 1.5 and varying Na_2O dosages of 4% and 8% by mass of binder was employed to activate the FCS and BS blend. The optimum M_s ratio depends on the precursor type and the purity of activator solutions. Hence, a set of preliminary tests were conducted and the optimum M_s ratio was found as 1.5. Subsequently, Na_2O dosage was altered from a lower ratio (4%) to a higher ratio (8%) in order to elucidate its effect. The mortar samples were manufactured using water-to-binder (w/b) and sand-to-binder ratios (s/b) of 0.4 and 2.0, respectively, which also provided reasonable flow values higher than 100%. It should be noted that the total water content was calculated considering the amount of water presented in liquid Na_2SiO_3. The paste mixes were also manufactured (without adding sand) with the similar design parameters to investigate rheological and microstructural properties. The alkaline solutions were prepared by combining the designated amount of water NaOH and liquid Na_2SiO_3 solutions. The alkaline solution was stirred to dissolve NaOH pellets with liquid Na_2SiO_3 and tap water and wrapped with a stretch film to prevent evaporation and carbonation. Subsequently, the alkaline solution was left to cool and then combined with the blend of FCS and BS in a mixer bowl. The sand was also gradually added to mixer mold within 30 s, and mixing was continued for up to 5 min to achieve homogenous mixtues. The fresh paste and mortars were poured into pertinent molds and vibrated to enable proper compaction. The hardened samples were removed from the molds after 24 h of casting and kept under standard conditions in a chamber at 22 ± 1 °C and 55 ± 2% relative humidity (RH) until the specified testing age. For mortar mixtures, the mix IDs presented in Table 2 are categorized with the letters “F” and “N”

Table 1
XRF results of FCS and BS.

Precursor	Oxide components (wt %)														
	MgO	SiO_2	Al_2O_3	Cr_2O_3	K_2O	Fe_2O_3	Na_2O	CaO	Mn_2O_3	TiO_2	P_2O_5	SO_3	Cl^-	LOI[a]	Others
FCS	34.85	34.19	20.50	2.92	0.22	1.69	0.28	1.62	0.22	0.01	0.01	0.17	0.01	0.5	2.80
BS	5.00	39.00	12.50	–	0.20	1.00	0.60	37.50	–	–	–	0.20	–	0.2	3.80

[a] Loss on ignition (LOI).

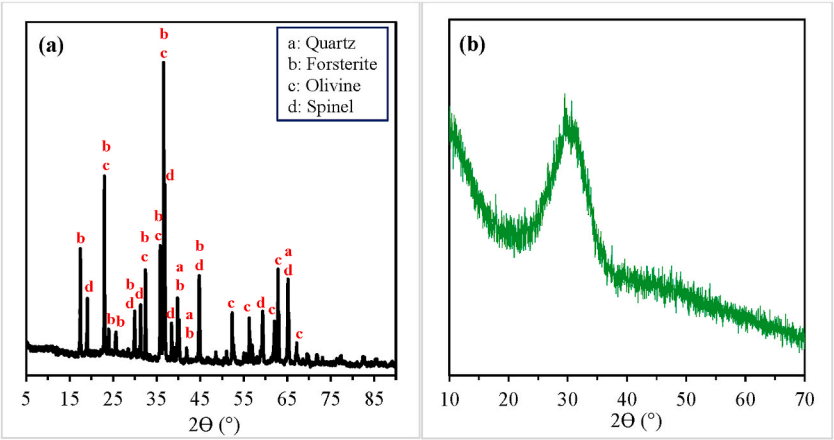


Fig. 2. XRD phases: (a) FCS and (b) BS.

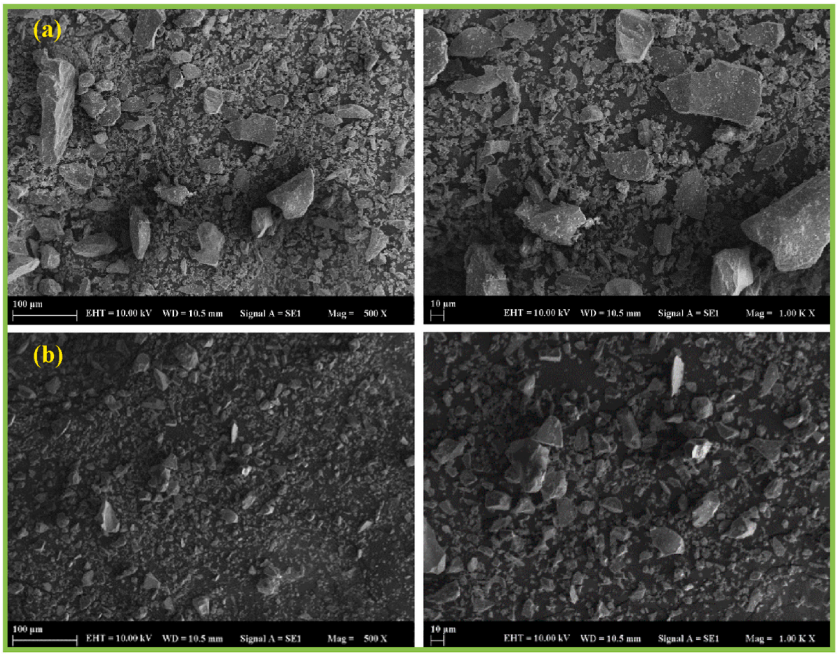


Fig. 3. SEM micromorphology of: (a) FCS and (b) BS.

Table 2
The design parameters of the mortar mixtues.

Paste mixes							Mortar mixes						
Mix ID	FCS (wt %)	BS (wt %)	Na_2O (wt %)	w/b	s/b	Ms ratio	Mix ID	FCS (wt %)	BS (wt %)	Na_2O (wt %)	w/b	s/b	Ms ratio
P0–N4	0	100	4	0.4	–	1.5	F0–N4	0	100	4	0.4	2	1.5
P10–N4	10	90	4	0.4	–	1.5	F10–N4	10	90	4	0.4	2	1.5
P20–N4	20	80	4	0.4	–	1.5	F20–N4	20	80	4	0.4	2	1.5
P30–N4	30	70	4	0.4	–	1.5	F30–N4	30	70	4	0.4	2	1.5
P0–N8	0	100	8	0.4	–	1.5	F0–N8	0	100	8	0.4	2	1.5
P10–N8	10	90	8	0.4	–	1.5	F10–N8	10	90	8	0.4	2	1.5
P20–N8	20	80	8	0.4	–	1.5	F20–N8	20	80	8	0.4	2	1.5
P30–N8	30	70	8	0.4	–	1.5	F30–N8	30	70	8	0.4	2	1.5

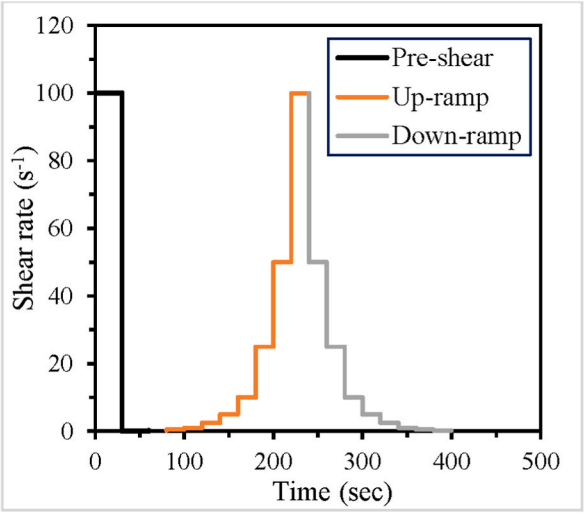


Fig. 4. The rheological test procedure.

representing "FCS" and "Na_2O dosage" followed by numbers denoting either the FCS percentage or the Na_2O dosage, respectively. For instance, "F30–N8" represents the mixes containing 30% FCS and 70% BS activated with alkaline solution having 8% Na_2O dosage. Similarly, the paste mixes were designated according to their FCS replacement ratios and Na_2O dosages and were coded using 'P' instead of 'F' to distinguish them from mortar mixes.

2.3. Experimental procedures

2.3.1. Fresh properties

The plastic viscosity and yield stress of the paste mixes were investigated to determine the effects of FCS replacement and Na_2O dosage on the fresh properties. The rheological measurement was carried out using a rotational rheometer (Anton Paar Rheolab QC) equipped with a temperature controlling system. A four-blade vane blender measurement apparatus (40 mm in length and 11 mm in diameter) was employed to blend the paste mixes. The implemented rheological procedure on paste samples is depicted in Fig. 4. Each shear rate was put on for 20 s in order to determine the shear. The rheology measurements were conducted right after the stirring of the fresh paste mixes into the mixer bowl and the temperature was kept at 20 °C during measurements for all pastes. The test technique described in ASTM C1437 standard was carried out to determine the flow values of fresh mortar mixtures using a truncated cone mold. The spreading diameters of the mortar samples were recordedand the flow values were presented as the percentage increment of the mortar diameter compared to the original base of the truncated cone mold (10 cm).

The setting times of fresh paste mixes were determined using Vicat apparatus. The approach outlined in ASTM C191 standard was pursued ignoring the specification of standard consistency since the w/b ratio of each mix was kept constant.

2.3.2. Physical tests

The water absorption and volume of permeable pores (VoPP) of the mortar samples were determined as per ASTM C642 standard with a modification during oven drying stage of the test. After curing for 28 days, the mortar samples were dried for about 24 h in a ventilated oven at 60 °C instead of 110 ± 5 °C in order to prevent the deterioration of the matrix phases of mortar samples due to the thermal drying [36]. The samples were then cooled down to the ambient temperature and the oven dry mass (A) was recorded. Subsequently, the samples were immersed in a water tank for 48 h. After removing the samples from water, the saturated and surface dried (SSD) mass (B) was recorded. The mortar specimens were then placed in the boiling water and kept for 5 h. The samples were allowed to cool for at least 14 h in water to reach ambient temperature. Finally, SSD mass and the apparent mass in water after boiling were recorded as (C) and (D), respectively. The water absorption and VoPP of mortars were calculated using Eqs. (1) and (2).

$$Water\ absorption\ (\%) = \frac{B - A}{A} \times 100 \tag{1}$$

$$Volume\ of\ permeable\ pores\ (\%) = \frac{C - A}{C - D} \times 100 \tag{2}$$

The open porosity of mortar samples was determined using the method proposed by Ref. [37]. The specimens were heated in an oven (60 °C) until steady mass (W_{od}) and later placed in a sealed container. The pressure of the container was steadily set to 2 ± 0.7 kPa applying a vacuum pump. The vacuum was operated at constant pressure for 2 h to completely remove the air from the open voids of the samples. Subsequently, deionized water was added progressively to the container to fully submerge all samples under the constant vacuum pressure of 2 ± 0.7 kPa. The pressure was then decreased to atmospheric pressure and the specimens were kept in water for 24 h. In the final step, SSD mass (W_{sa}) and the mass in water (W_{sw}) were recorded. The open porosity of mortars was calculated using Eq.

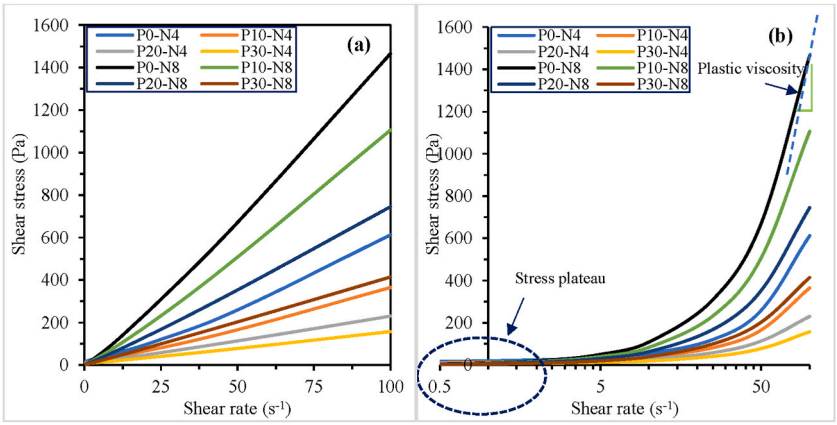


Fig. 5. The flow curves (shear stress-shear rate graphs) of paste mixes in the: (a) linear axis and (b) logarithmic axis (stress pleteau approach).

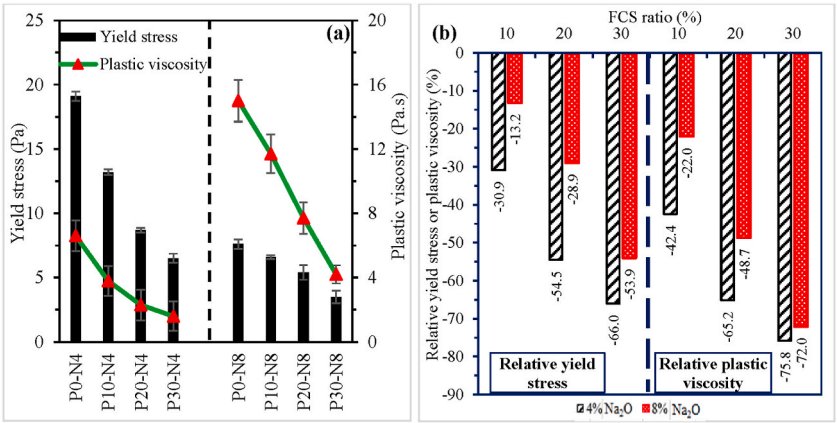


Fig. 6. (a) The obtained rheological parameters (plastic viscosity and yield stress) of alkali-activated paste mixtures and (b) the change in the yield stress or plastic viscosity of alkali-activated pastes with varying FCS ratio.

(3).

$$Open\ porosity\ (\%) = \frac{W_{sa} - W_{od}}{W_{sa} - W_{sw}} \times 100 \tag{3}$$

The water sorptivity of mortar samples was evaluated at the age of 28 days according to ASTM C1585 standard. The cylindrical mortar samples having dimensions of 100 mm diameter and 50 mm thickness were submerged in water until saturation. The samples were subsequently placed in a chamber and kept under constant temperature and RH of 50 ± 1 °C and 80 ± 3%, respectively. The specimens were then stored in airtight containers at 23 ± 1 °C for 15 days. The lateral surfaces of the samples were then coated with a paraffin wax. The sorptivity test was initiated by placing the samples in containers where the water level was about 1 mm above the bottom of the sample. The mass readings were taken for up to 6 h at specified intervals indicated in the ASTM C1585 standard, and daily measurements were taken until the 8th day.

2.3.3. Compressive strengh and pH evolution

The compressive strength was determined on three identical cubic samples of 50 mm dimensions at 3, 7, and 28 days. The average values were reported for each mix at specified testing age. The pH values were studied to establish their relationship with the compressive strength development. The pH values were determined on paste samples after crushing them into powder with a size <75 μm. The powder samples were dissolved in distilled water with a powder to water ratio of 5:1 and stirred at 1200 rpm for 15 min using a magnetic stirrer. The resulting solution was filtered with a vacuum filter, and the pH values were measured at 3, 7, and 28 days with an accuracy of ±0.01 using Hanna pH meter instrument.

2.3.4. Microstructural investigation

The paste specimens were poured into the falcon tubes of 50 ml and maintained in a chamber at 22 ± 1 °C and 55 ± 2 RH to examine the microstructural properties. After 28 days, the paste samples were soaked in acetone to prevent further hydration reactions, and thin slices and powder samples were taken to carry out SEM and XRD analysis, respectively. The microstructural

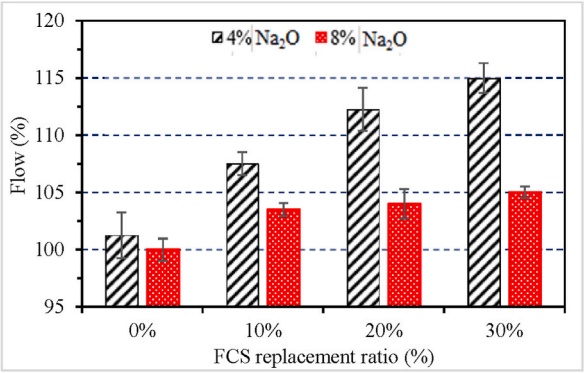


Fig. 7. The flow table test results of mortar samples.

properties of alkali-activated paste mixes was investigated with SEM analysis combined with Energy dispersive X-ray spectroscopy (EDS) using Zeiss EVO® LS 10 SEM device. The XRD analysis was performed using PANalytical X'Pert PRO diffractometer to identify the mineralogical phases for the selected paste mixes. The diffraction pattern was recorded with a step size of 0.017° and a scan range of 5–90° (2Θ). SEM and XRD analysis are also performed on the raw materials (FCS and BS).

3. Result and discussion

3.1. Fresh state properties

3.1.1. Rheology

The rheological properties of alkali-activated paste mixes were investigated considering the effects of FCS and Na_2O dosage. The down-ramp of the shear stress-rate plots was considered while determining the rheological parameters. The flow curves of the paste samples are plotted in Fig. 5 as both linear and logarithmic axis to understand the best mathematical rheological model. The stress plateau approach was adopted to determine the plastic viscosity and yield stress values. Hence, the flow curves were drawn on a logarithmic axis for better resolution at low shear rates. The plateau-like flat area represents the yield stress value, whereas the slope of the linear curve between the shear rates of 25 s^{-1} and 100 s^{-1} on the flow curve describes the plastic viscosity. Shear-thinning behavior is defined as a drop in viscosity that causes floccules to break apart as a consequence of an increase in shear rate [38]. Fig. 6 shows the results of rheological parameters and the variation of these parameters depending on the FCS replacement ratio. As shown in Fig. 6, shear thinning behavior was observed for each mix similar to cementitious slurries, irrespective of the mix design [39,40].

The important factors that govern the rheological characteristics of alkali-activated binders are the alkali activator parameters such as Ms ratio, alkaline solution to binder ratio, and Na_2O dosage. The plastic viscosity of the examined paste mixes ranged between 1.6 and 15.0 Pa s. The rise in the Na_2O concentration from 4% to 8% significantly increased the plastic viscosity values of the pastes up to 235%, irrespective of the FCS content. Similar observations were previously reported by Refs. [41,42] on alkali-activated paste mixes. This observation can be ascribed to the higher alkaline solution viscosity resulting from the greater amount of silicate and Na^+ ions. It has been reported that the existence of colloidal Si–O–H–Na complexes on the order of 0.6 nm, which form clumps on the order of a few nanometers [42–44], elevates the viscosity of concentrated alkali silicate solutions. In addition, the amount or size of these colloidal complexes and clumps increases with an increase in the Si content and this decreases the presence of hydroxyl ions required to break the siloxan bonds [45], which induces higher solution viscosity. Besides, the increase in the Na_2O dosage increases the amount of Na^+ ions in the alkaline solution, which induces higher formation of Si–O–H–Na complexes by creating ion-dipole forces [46].

The increase in the Na_2O dosage consistently reduced the yield stress of the examined paste samples, irrespective of the FCS content. The influence of Na_2O dosage on the yield stress of BS-based silicate activated systems are reported to be complex [47]. In the case of lower M_s ratio (i.e., <0.8), an increase in the Na_2O dosage increases the yield stress. However, at higher M_s values (i.e., >1.2), the higher Na_2O dosage was found to induce lower yield stress [47], which is in line with the present study.

Another main parameter that affects the rheology of alkali-activated based systems is the precursor type. The precursor characteristics may influence the fluidity of mixes due to their properties such as particle size, particle shape, hydrophobic/hydrophilic nature, surface texture, and dissolved ionic species [18,48]. It is clearly observed that the incorporation of FCS consistently reduced both plastic viscosity and yield stress values of the pastes, which consequently improved the workability. The plastic viscosity values reduced from 6.6 Pa s to 1.6 Pa s for 4% Na_2O, and from 15 Pa s to 4.2 Pa s for 8% Na_2O when 30% of BS was replaced by FCS. The reduction in plastic viscosity was more than 70%. Similarly, in the case of 30% FCA replacement, the yield stress values decreased from 19.1 Pa to 6.5 Pa and 7.6 Pa–3.5 Pa compared to the mixes without FCS for 4% and 8% Na_2O dosages, respectively indicating a reduction of more than 54%, as illustrated in Fig. 6b. This beneficial impact of FCS on the rheological properties may be due to its distinct PSD and surface texture compared to BS. The coarser particle size of FCS may provide a higher free water content for same w/b ratio by reducing the water demand of mixes. The rheology test results are in well agreement with the flow table test results performed on mortar samples, in which the higher FCS replacement ratio increased the fluidity.

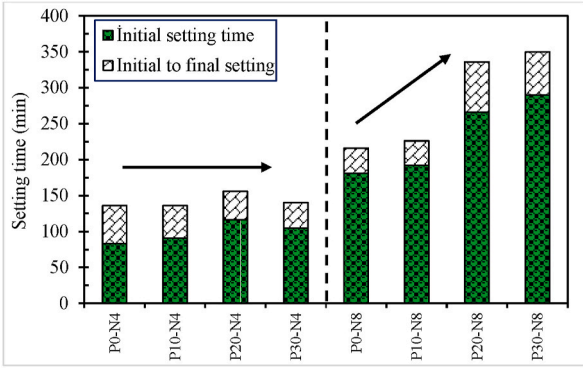


Fig. 8. The setting time results of alkali-activated paste mixes.

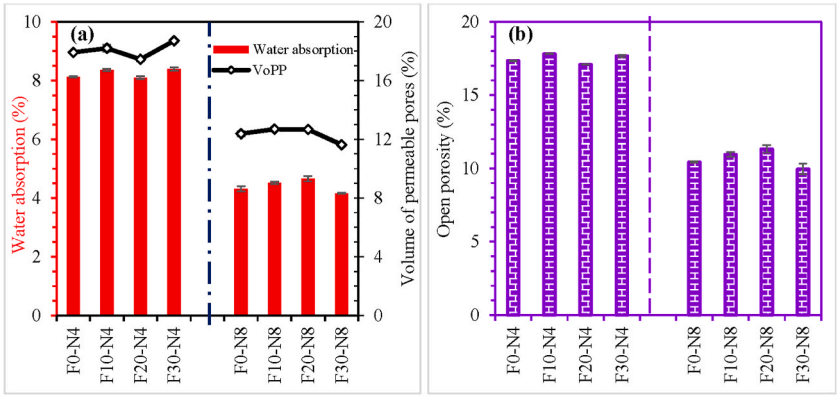


Fig. 9. The physical properties of mortar samples: (a) water absorption and VoPP (b) open porosity.

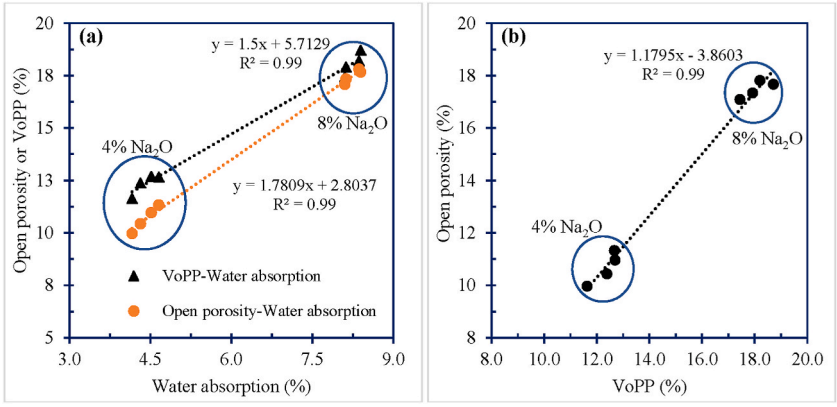


Fig. 10. The relationship between: (a) Open porosity or VoPP and water absorption (b) open porosity and VoPP.

3.1.2. Flow table test

Fig. 7 shows the effect of FCS replacement ratio and Na_2O dosage on the flowability of each mortar mix. The flow values of mortar mixes ranged between 100% and 115% which provided ease in molding. An increase in the FCS replacement ratio consistently increased the flow values, irrespective of the Na_2O dosage. This may be due to the coarser and broader particle size distribution of FCS compared to BS, which promotes a smaller specific surface area. The lower specific surface area of FCS causes fewer molecules of water to be encapsulated and moistens the particle surface, thereby increasing the amount of free water in the mixture and enhancing its flowability [49]. It was observed that this increase was more pronounced for mixes produced with 4% Na_2O dosage. The incorporation of 30% FCS increased the flow of mixes by 13.7% and 5.0% for the mixes containing 4% and 8% Na_2O dosages compared to the reference mixes without FCS, respectively. In addition, the flow values decreased by maximum of 10.0% with an increase in the Na_2O

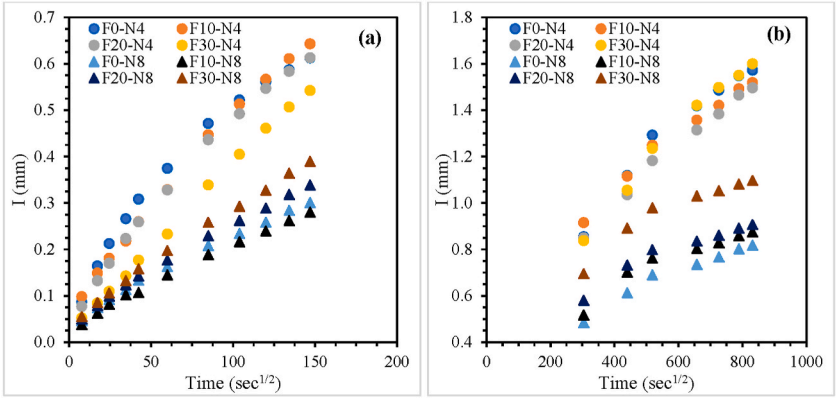


Fig. 11. The capillary sorptivity results of mortar mixes: (a) IS and (b) SS.

Table 3
The IS and SS of mortar samples.

Sample code	Initial sorptivity (mm/sec$^{0.5}$)	Secondary sorptivity (mm/sec$^{0.5}$)
F0–N4	0.0036	0.0013
F10–N4	0.0040	0.0011
F20–N4	0.0038	0.0012
F30–N4	0.0036	0.0014
F0–N8	0.0018	0.0006
F10–N8	0.0017	0.0006
F20–N8	0.0020	0.0006
F30–N8	0.0024	0.0007

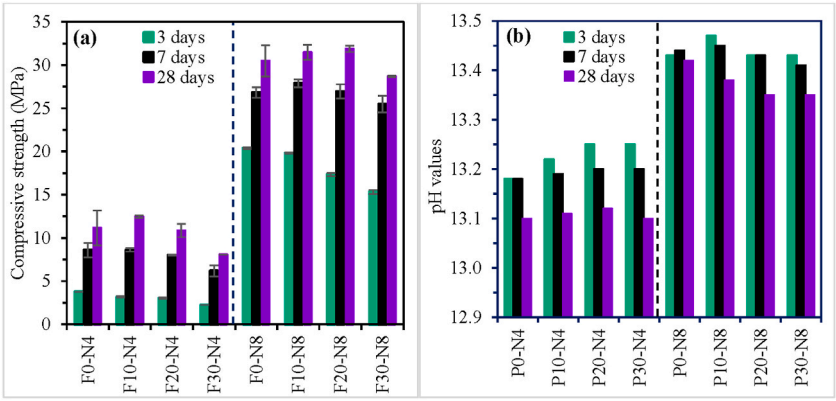


Fig. 12. (a) Compressive strength development of mortar mixes and (b) pH evolution of corresponding paste samples.

dosage from 4% to 8%. It is worth noting that, the amount of sodium silicate was increased proportionally to obtain a constant M_s ratio, with an increase in Na_2O dosage of the mixtures. Therefore, this flow reduction resulting from the higher Na_2O dosage is possibly due to the higher amount of silica content of the mixes produced with 8% Na_2O dosage (see Section 3.1.1). Similarly, it has been previously noted that the higher sodium silica content results in lower workability due to its highly viscous/sticky nature compared to NaOH [50].

3.1.3. Setting time

The effect of FCS substitution and Na_2O dosage on the setting time of paste mixes are depicted in Fig. 8. The initial setting time varied between 83 and 290 min, whereas the final setting times of pastes ranged between 136 and 350 min. In the case of 4% Na_2O dosage, FCS addition slightly increased the setting times and the initial and final setting times varied in a narrow range between 83-116 min and 136–156 min, respectively. However, for the mixes containing 8% Na_2O, the increase in FCS replacement ratio significantly prolonged the setting times. The initial and final setting times increased by about 60% with an increase in FCS substitution ratio. This can be credited to the higher dissolution capacity of BS at higher Na_2O dosage [51] compared to FCS due to the presence of higher calcium ions (Table 1) and to the amorphous characteristic of BS (Fig. 2). It has been reported that calcium ions accelerate the polycondensation reactions, which alleviate the formation of calcium-alumina-silicate-hydrate (C-A-S-H) gels, responsible for

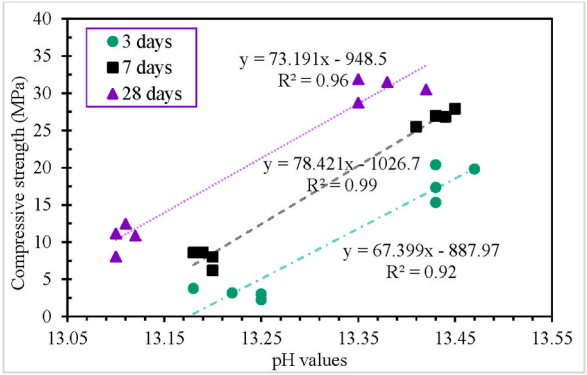


Fig. 13. The relationship between pH values and compressive strength.

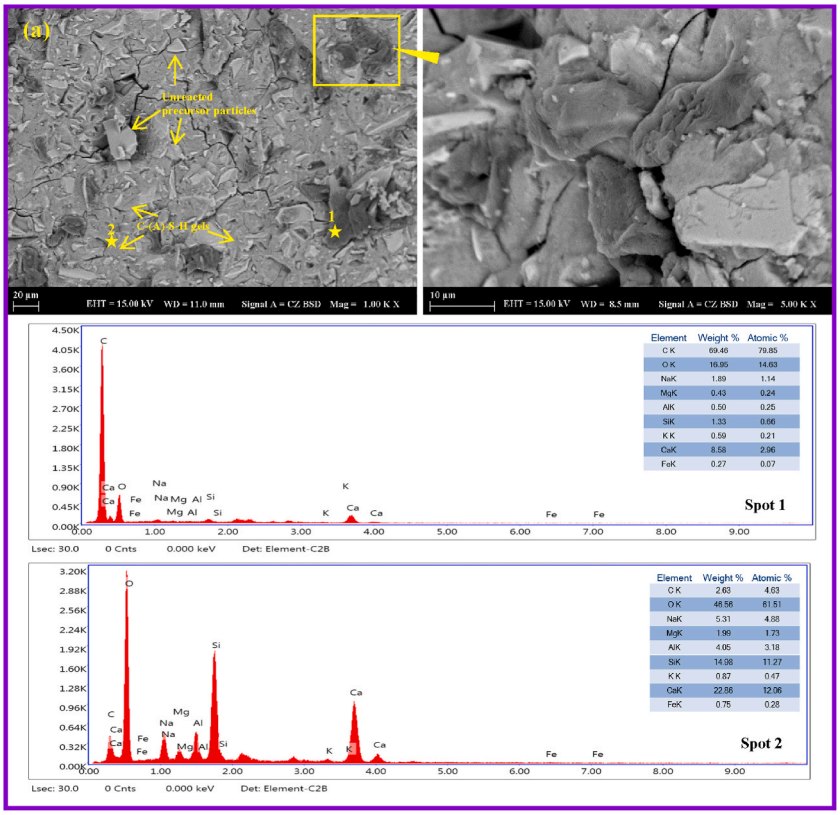


Fig. 14. SEM-EDS analysis of alkali-activated paste samples: (a) P0–N4, (b) P10–N4, (c) P30–N4, (d) P0–N8, (e) P10–N8, and (f) P30–N8.

hardening [52]. The extended setting time provided by the addition of FCS might be advantageous especially for on-site applications requiring longer casting durations and in hot weather conditions.

The effect of Na_2O dosage on the setting time was significant and an increase in Na_2O dosage prolonged the initial and final setting times of pastes by up to 176% and 150%, respectively, irrespective of the FCS content. It was previously reported that the higher Na_2O dosage yields lower setting time due to the accelerated polycondensation and rapid formation of the binding phases [53]. On the other hand, Adam et al. [54] revealed that this drop in setting time was reversed after a certain Na_2O ratio (7%), and a further rise in Na_2O dosage extended the setting, similar to this study.

3.2. Physical properties

3.2.1. Water absorption, volume of permeable pores, and open porosity

Fig. 9 shows the water absorption, VoPP, and open porosity values of mortar samples at 28 days. The test results indicated that for a

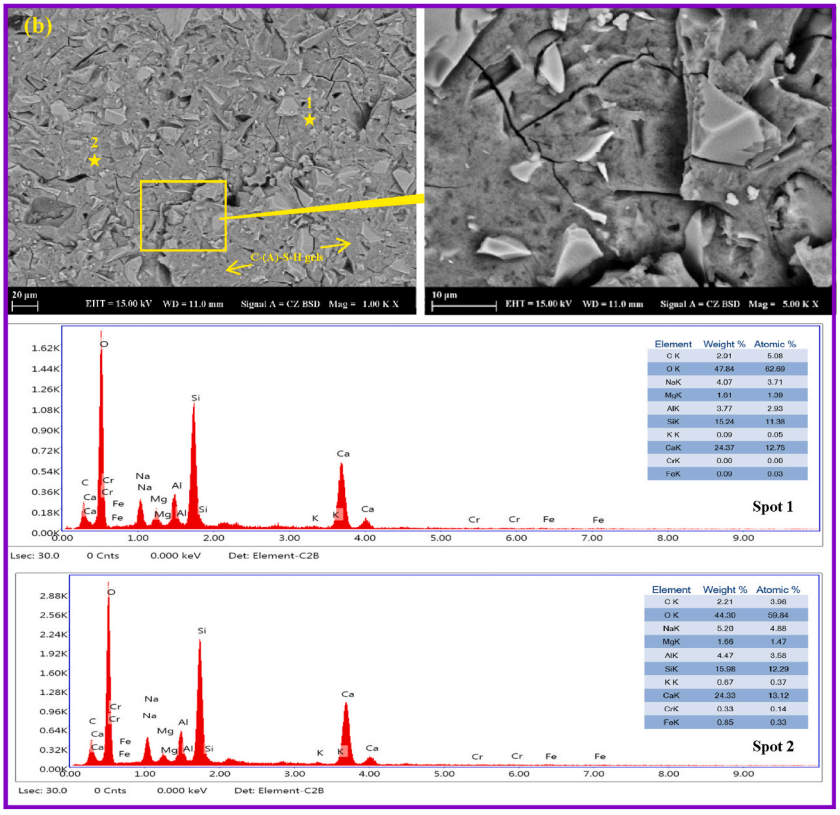


Fig. 14. (*continued*).

fixed Na_2O dosage the physical properties of the samples slightly changed with an increase in FCS ratio. The water absorption, VoPP, and the open porosity of the mortar mixes varied in the range between 8.1 and 8.4%, 17.4–18.7%, and 17.1–17.8% for 4% Na_2O dosage, respectively. However, these values significantly reduced at higher Na_2O dosage. The absorption values of mortars almost halved and the VoPP and the open porosity reduced more than 30% with a higher Na_2O dosage. The reduced water absorption and porosity implies that the mortar specimens have denser structure due to enhanced gel formation with increased Na_2O dosage. This has been verified by SEM-EDS and XRD analysis and further discussed in Section 3.4. The overall test results indicated that the FCS replacement up to 30% had no significant impact on the physical properties of the BS-based mortars, on the other hand increasing Na_2O dosage resulted in significant reduction on the tested physical parameters.

Fig. 10 depicts the relationship between physical test results. It is found that water absorption and both VoPP or open porosity have statistically significant relationships ($R^2 > 0.99$) in which the lower VoPP or open porosity yields lower water absorption and vice versa.

3.2.2. Capillary sorptivity

The sorptivity of mortar samples as a function of square root of time are depicted in Fig. 11. The sorptivity behavior of specimens was divided into two categories: initial sorptivity (IS) and secondary sorptivity (SS). The slopes of the first (1 min–6 h) and second (1 day–8 days) sections of the graphs were used to determine the IS and SS values, respectively, and the results are presented in Table 3. The IS results from the quick absorption of capillary pores, whereas the gradual filling of entrained or entrapped air pores and microcracks induces the SS [55]. The results indicate that the variation in the IS and SS with the incorporation of FCS was generally insignificant. The IS values of the mortar mixes were between 0.0036 and 0.0040 $mm/s^{0.5}$ and 0.0017 and 0.0024 $mm/s^{0.5}$ for Na_2O dosage of 4% and 8%, respectively. The SS values ranged among 0.0006 and 0.0014 $mm/s^{0.5}$. The increase in Na_2O dosage to 8% resulted in significantly lower sorptivity values. Capillary sorptivity is intimately linked to total porosity, pore structure, and tortuosity. The higher tortuosity of the C-A-S-H type gels [56,57] that are copiously produced in higher alkaline ambient in alkali-activated specimens may be a reason for the smaller capillary water absorption. In addition, lower open porosity and VoPP values of the mixes with increasing Na_2O dosage may also explain the lower sorptivity of these specimens.

3.3. Compressive strength and pH evolution

The compressive strength results and the pH values determined at 3, 7, and 28 days are shown in Fig. 12. The compressive strength of each mix consistently increased with elapsed curing age. The F30–N4 mix had the lowest compressive strength of 8.1 MPa, whereas F20–N8 specimen achieved the highest strength of 31.9 MPa at 28 days. It can be observed from Fig. 11a that the compressive strength

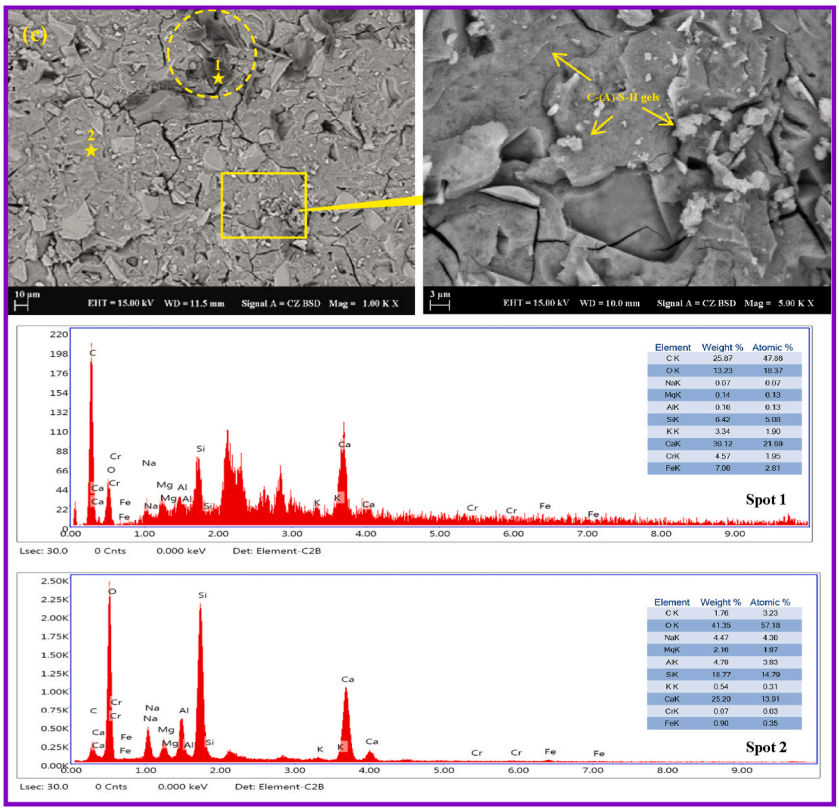


Fig. 14. (*continued*).

of mortars significantly increased in the range between 152% and 254% with an increase in the Na_2O dosage regardless of FCS replacement ratio. This is in line with the other studies, as it has been reported that the increase in Na_2O concentration induces the formation of further OH^- ions (Fig. 11b), which in turn raises the dissolution of silicon and calcium ions, therefore increasing the synthesis of denser reaction products such as C–S–H and C-A-S-H, which consequently improves the mechanical performance [58,59].

The results also indicated that the incorporation of FCS up to 20% had no significant effect on the compressive strength, as the mixes achieved comparable strength values at 7 and 28 days. In the case of 8% Na_2O dosage, the incorporation of 10 and 20% FCS slightly increased the compressive strength by 3% and 5% at 28 days, respectively, compared to F0–N8 mix. However, the inclusion of 30% FCS (F30–N8) led to a slight reduction of about 6% compared to F0–N8. Nevertheless, the preservation of compressive strength indicates that the utilization of FCS up to 30% is beneficial for BS-based alkali-activated systems. Even though its crystalline structure and lower calcium content, the wider PSD of FCS might have improved the particle packing property that positively affected the mechanical properties.

In order to elucidate the strength variation process, the pH values of the paste specimens were quantified at various curing periods. Test results showed that the pH values of paste mixes at 3, 7 and 28 days ranged between 13.18 and 13.47, 13.18–13.45, and 13.10–13.42, respectively. It was found that the pH values of the mixes consistently reduced with the progressive curing age which is mainly due to the formation of gel type reaction products. At the early stage of reactions, alkaline solution (NaOH and Na_2SiO_3) contributes significant amount of OH^- ions and increases the pH value of the AAM system. In addition, the oxide compounds of BS and FCS dissolves when they interact with water to generate compounds such as $Ca(OH)_2$ and $Mg(OH)_2$, which further increases the pH of the system [60]. However, the polycondensation reactions progresses with curing age and these hydroxyl compounds are consumed to synthesize reaction products such as C-A-S-H and/or magnesium aluminum silicate hydrate (M-A-S-H) and which consequently decreases the pH value of the pastes. On the other hand, the increase in the Na_2O dosage remarkably increased the pH value of the mixes, which is due to the extra hydroxyl ions coming from the alkaline solution. Furthermore, considering the effect of FCS on pH values, two distinct behaviors were detected depending on the Na_2O dosage. In the case of 4% Na_2O, the FCS inclusion consistently increased the pH of the samples at both early and later ages. However, when 8% Na_2O was used, similar pH values were obtained with increasing FCS ratio at early ages, whereas pH values decreased with increasing FCS ratio at 28 days. This may indicate that FCS contributes more to gel formation when used in a higher alkaline ambient (i.e., high pH of pore solution).

Fig. 13 shows the linear relationship between pH values and compressive strength of the alkali-activated mixes with a satisfactory R^2 value of greater than 0.92 and the higher pH values resulted in higher mortar compressive strength.

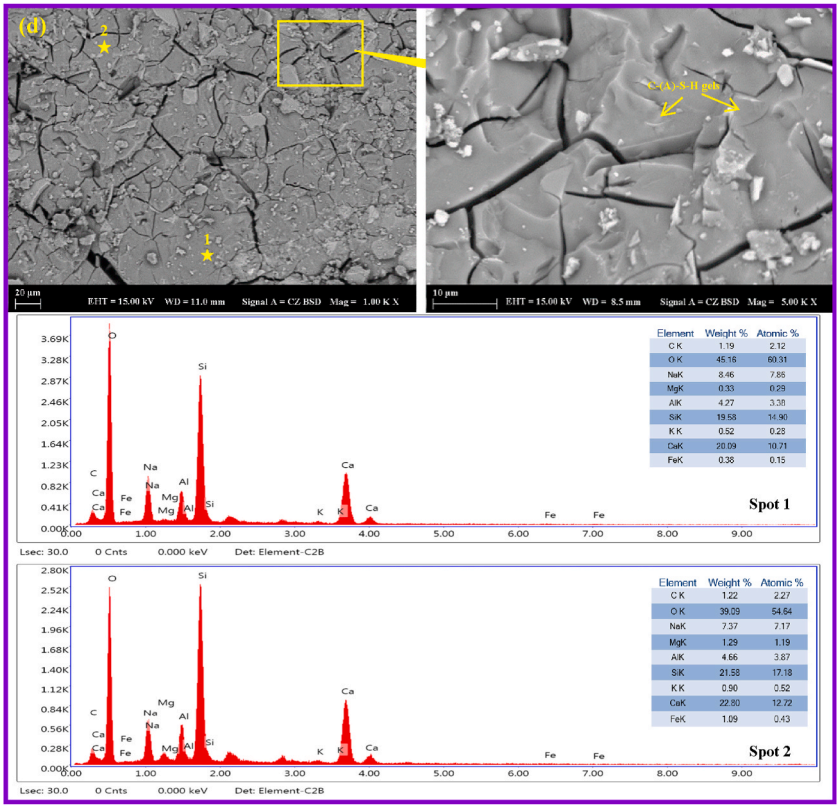


Fig. 14. (*continued*).

3.4. Microstructural investigation

3.4.1. SEM-EDS analysis

Fig. 14 shows the microstructural morphology of alkali-activated paste samples. SEM analyses were conducted with backscattered mode to distinguish unreacted particles and gel phases under the magnifications of ×1000 and × 5000. A total of 5 points were selected for each investigated sample in order to conduct EDS analysis and 2 representative analysis points were presented in Fig. 14 for each tested sample. The mean atomic ratios such as Ca/Si and Si/Al were calculated considering the matrix phase by excluding the points of unreacted particles, and the results are shown in Table 4. SEM analysis results showed that micromorphology of the paste mixes altered with the change of Na_2O dosage, whereas the addition of FCS slightly affected the general morphology. It was observed that the unreacted particles corresponding to FCS and BS are homogeneously dispersed throughout the studied areas. In addition, the increase in the Na_2O dosage reduced the amount of unreacted precursor particles, which indicates improved hydration reactions. It was also observed that the mixes containing 8% Na_2O dosage exhibited higher amount of microcracks which is possibly due to the higher shrinkage characteristics of BS-based AAM mixes at higher alkaline ambient [61]. The EDS analysis revealed that C, O, Ca, Si, Al, Mg, Na, and Fe elements were generally detected for all mixes. The darker areas (dashed circles in Fig. 14) observed in some mixes were rich in C, O, and Ca elements and possibly show the formation of $CaCO_3$ and the number of these areas decreased with higher Na_2O dosage. In addition, several white spots with particle sizes between 3 and 5 μm were identified in P10–N8 and P30–N8 mixes (Fig. 14e and f). The XRF and XRD analyses of raw FCS reveal that these spots might be metallic iron or iron oxide, as also verified by the EDS analysis. However, these particles were not detected in the paste samples prepared with 4% Na_2O containing FCS which may indicate that FCS particles could further dissolve under higher alkaline conditions.

The EDS results showed that Ca/Si ratio of the mixes activated with 4% Na_2O dosage varied between 0.95 and 1.16, whereas this ratio decreased and ranged between 0.75 and 0.90 for the mixes with 8% Na_2O dosage. On the other hand, the incorporation of FCS insignificantly altered the Ca/Si ratio. The obtained Ca/Si ratios of the present study were compatible with the ratio of C-(A)-S-H gel, which was previously reported in the literature [62]. The potential C-(A)-S-H gel regions were identified in Fig. 14 according to the Ca/Si ratio using EDS data. It was previously shown that the Si/Al ratio play a significant role in the strength development and an increase in the Si/Al ratio generally yields higher compressive strength [16]. As shown in Fig. 15, linear relationship is established between Si/Al and the compressive strength which shows that an increase in the Na_2O dosage results in an increase in Si/Al atomic ratio and compressive strength.

3.4.2. XRD analysis

Fig. 16 depicts the XRD patterns of the paste mixes. The increase in the FCS ratio consistently increased the crystallinity of the

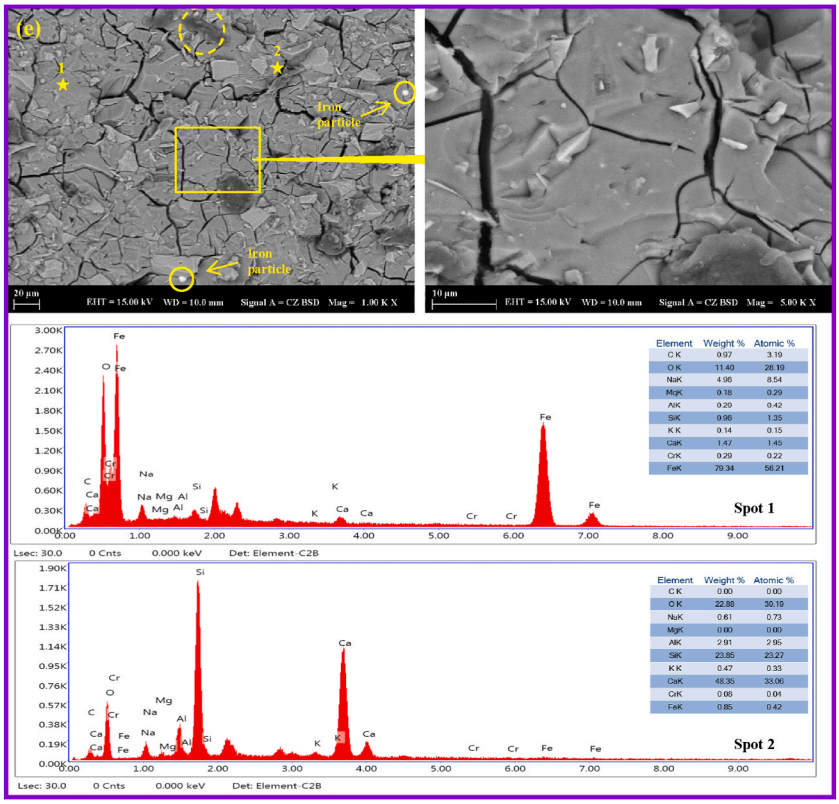


Fig. 14. (*continued*).

detected phases. The major peaks were identified as spinel, forsterite, calcium aluminum silicate ($Ca_3Al_2Si_2$) (#PDF 01-083-1278), magnesium aluminum silicate ($Al_2Mg_3O_{18}Si_6$) (#PDF 01-076-0537), and calcite ($CaCO_3$) (#PDF 00-047-1743) for the mixes containing FCS. However, P0–N4 and P0–N8 mixtures exhibited highly amorphous diffraction patterns with a single broad peak located at around 29.68° 2Θ, as previously detected in the XRD spectra of raw BS. This peak was identified as calcium aluminum silicate for P0–N4 and P0–N8, which may correspond to the formation of strength-giving gels such as C–S–H, and C-A-S-H due to the abundant presence of calcium in raw BS. Magnesium aluminum silicate phases were also detected at the same peak (29.68° 2Θ) with the incorporation of FCS. The peaks of magnesium aluminum silicate may indicate the formation of M-A-S-H type gel with the addition of FCS. The presence of high amount of magnesium and aluminum and low amount of calcium in FCS may have led to the formation of M-A-S-H gels which were detected at around 29.5°, 31.5°, 32.4°, 36.9°, and 44.8° 2Θ. In the case of 10% FCS replacement, forsterite and spinel peaks emerged, which come from the raw FCS at around 18°, 23°, 37°, 40°, and 65° 2Θ. Furthermore, the intensity of spinel and forsterite peaks increased with an increase in FCS content.

The increase in the Na_2O dosage generally decreased the peak intensities of crystalline phases for their corresponding FCS replacement ratio. The reduced forsterite and spinel peaks implies that the reaction of FCS particles enhance in higher alkaline ambient. This finding can be corroborated with the SEM images of P10–N8 and P30–N8 (Fig. 14e and f), in which the dissolved iron oxide particles were observed.

4. Conclusions

The purpose of this study is to investigate the fresh, physical, mechanical, and microstructural properties of FCS incorporated alkali-activated BS-based paste and mortar mixtures. The effects of FCS replacement and Na_2O dosage were discussed. The key outcomes of this study are listed below.

- FCS substitution improved the fresh state properties of the paste and mortar mixes by reducing the plastic viscosity and yield stress values and increasing both the initial and final setting times. Thus, the utilization of higher FCS content can be favorable to solve the stickiness and fast setting problem of BS-based AAMs.
- The incorporation of FCS up to 30% had no adverse effect on the water absorption, VoPP, open porosity and sorptivity of the mortars without compromising compressive strength. In addition, the increase in Na_2O dosage improved the physical and mechanical properties of mortars significantly.
- The pH values indicated that the alkalinity of the paste samples decreased with the elapsed curing age due to the formation of reaction products. The increase in FCS ratio increased the pH values of the samples when 4% Na_2O was used. In contrast, this trend

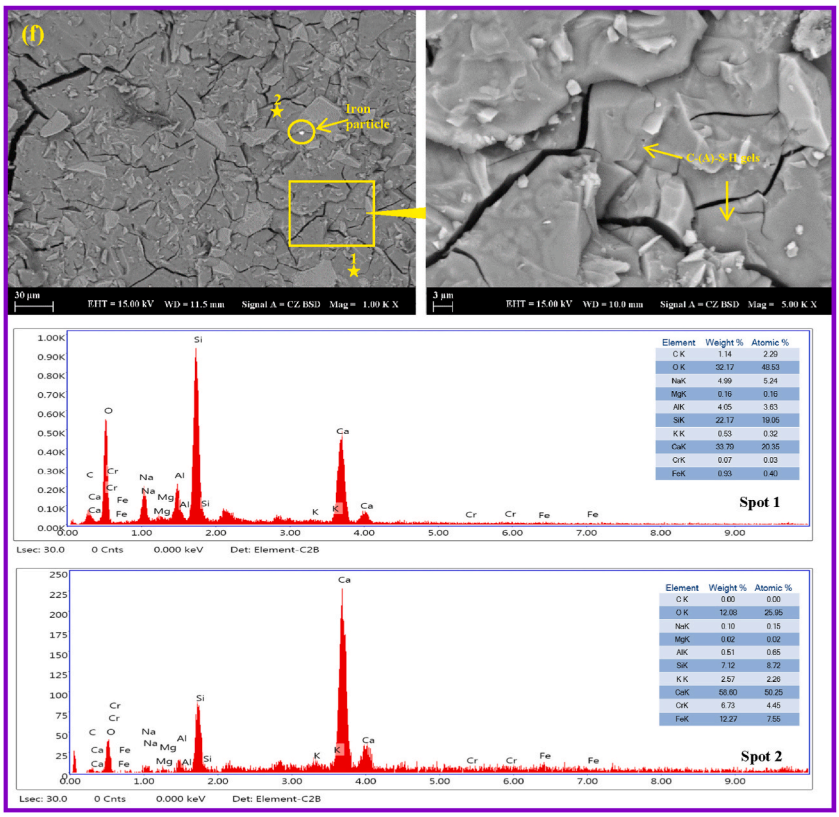


Fig. 14. (*continued*).

Table 4
The average EDS atomic ratios of the mixes.

Sample ID	Ca/Si ratio	Si/Al ratio	Na atomic percentage (%)
P0–N4	1.16 ± 0.12	3.68 ± 0.19	4.83 ± 0.07
P10–N4	1.09 ± 0.04	3.66 ± 0.32	4.29 ± 0.82
P30–N4	0.95 ± 0.01	3.89 ± 0.15	4.85 ± 0.54
P0–N8	0.75 ± 0.03	4.42 ± 0.02	7.95 ± 0.82
P10–N8	0.90 ± 0.15	4.46 ± 0.55	7.31 ± 0.20
P30–N8	0.90 ± 0.16	4.72 ± 0.74	7.55 ± 1.10

was reversed in case of using 8% Na_2O dosage, and the pH values decreased with the addition of FCS, which indicates that the contribution of FCS on the alkali-activation process is higher in higher alkaline environment.

- Based on the microstructural and mineralogical investigations, the increase in the Si/Al atomic ratio was found to be beneficial for the compressive strength of the mixes. The main crystalline phases were detected as forsterite, spinel, calcium alumina silicate, and magnesium alumina silicate. The formation of latter two signifies the existence of C-A-S-H and M-A-S-H gels. In addition, the major reaction product was found as C-A-S-H gels in the mixes, whereas FCS addition led to an increase in the crystalline products and formation of M-A-S-H gels.
- Overall, the utilization of FCS up to 30% in alkali-activated BS-based mixtures was found to be beneficial since it facilitated flowability, extended setting times to an appropriate level enabling on-site applications, and did not adversely affect the mechanical and physical properties of the mortar mixes. The resulting mortar mixes containing FCS can be utilized in the execution of structural or non-structural elements for general use in construction that require compressive strength around 30–35 MPa. The utilization of FCS in BS-based AAM systems suggests a sustainable solution by reducing its impact on the environment without sacrificing the physical and mechanical properties.

CRediT author statement

Nausad Miyan: Software, validation, formal analysis, writing-review and editing; **Tarik Omur**: Software, validation, investigation, data curation, writing-original draft preparation; **Nihat Kabay**: Conceptualization, methodology, software, validation, formal

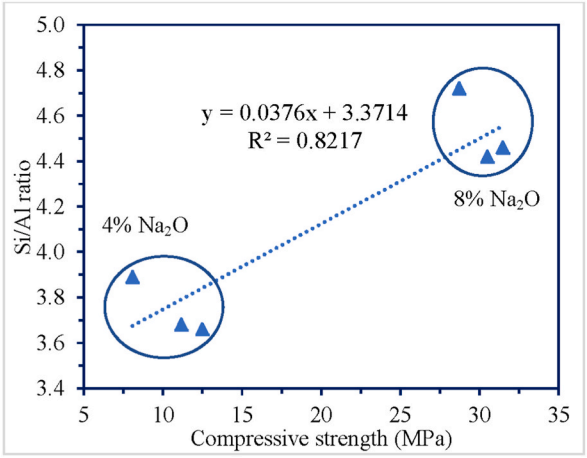


Fig. 15. The relationship between Si/Al atomic ratios and compressive strength.

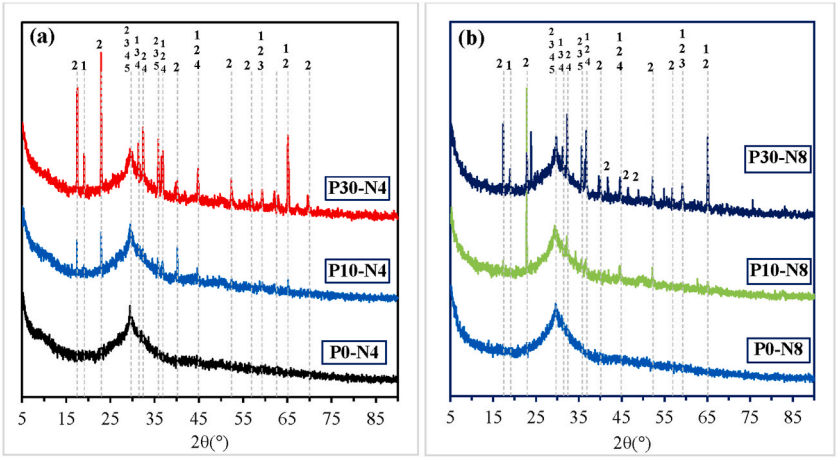


Fig. 16. The XRD patterns of: (a) P0–N4, P10–N4 and P30–N4 and (b) P0–N8, P10–N8 and P30–N8 (1: spinel, 2: forsterite, 3: calcium aluminum silicate, 4: magnesium aluminum silicate, and 5: calcite).

analysis, investigation, writing-original draft preparation, writing-review and editing, supervision; **Burak Birol**: Resources, writing-review and editing.

Declaration of competing interest

The authors declare that they have no known competing financial interests or personal relationships that could have appeared to influence the work reported in this paper.

Data availability

Data will be made available on request.

Acknowledgments

The authors are grateful for the support of Eti Krom A.Ş. (Elazığ, Türkiye) for procuring the ferrochrome slag utilized in this work.

References

[1] K. Al-Jabri, H. Shoukry, I.S. Khalil, S. Nasir, H.F. Hassan, Reuse of waste ferrochrome slag in the production of mortar with improved thermal and mechanical performance, J. Mater. Civ. Eng. 30 (2018), 04018152.
[2] K.S. Al-Jabri, Research on the use of Ferro-Chrome slag in civil engineering applications, in: MATEC Web of Conferences, EDP Sciences, 2018, 01017.
[3] M. Alwaeli, J. Nadziakiewicz, Recycling of scale and steel chips waste as a partial replacement of sand in concrete, Construct. Build. Mater. 28 (2012) 157–163.

[4] A. Sedaghatdoost, K. Behfarnia, M. Bayati, M. sadegh Vaezi, Influence of recycled concrete aggregates on alkali-activated slag mortar exposed to elevated temperatures, J. Build. Eng. 26 (2019), 100871.
[5] B.A. Akinyemi, P.A. Alaba, A. Rashedi, Selected performance of alkali-activated mine tailings as cementitious composites: a review, J. Build. Eng. 50 (2022), 104154.
[6] A. Neves, R. Godina, S.G. Azevedo, J.C.O. Matias, A comprehensive review of industrial symbiosis, J. Clean. Prod. 247 (2020), 119113.
[7] E.A.B. Cárcamo, R. Peñabaena-Niebles, Opportunities and challenges for the waste management in emerging and frontier countries through industrial symbiosis, J. Clean. Prod. (2022), 132607.
[8] A. Ferraro, V. Ducman, F. Colangelo, L. Korat, D. Spasiano, I. Farina, Production and characterization of lightweight aggregates from municipal solid waste incineration fly-ash through single-and double-step pelletization process, J. Clean. Prod. 383 (2023), 135275.
[9] A. Ferraro, F. Colangelo, I. Farina, M. Race, R. Cioffi, C. Cheeseman, M. Fabbricino, Cold-bonding process for treatment and reuse of waste materials: technical designs and applications of pelletized products, Crit. Rev. Environ. Sci. Technol. 51 (2021) 2197–2231.
[10] N. Sahu, A. Biswas, G.U. Kapure, A short review on utilization of ferrochromium slag, Miner. Process. Extr. Metall. Rev. 37 (2016) 211–219.
[11] P.H. Kumar, A. Srivastava, V. Kumar, M.R. Majhi, V.K. Singh, Implementation of industrial waste ferrochrome slag in conventional and low cement castables: effect of microsilica addition, Journal of Asian Ceramic Societies 2 (2014) 169–175.
[12] P.K. Acharya, S.K. Patro, Utilization of ferrochrome wastes such as ferrochrome ash and ferrochrome slag in concrete manufacturing, Waste Manag. Res. 34 (2016) 764–774.
[13] S.K. Nath, Geopolymerization behavior of ferrochrome slag and fly ash blends, Construct. Build. Mater. 181 (2018) 487–494.
[14] S. Chatterji, Mechanism of expansion of concrete due to the presence of dead-burnt CaO and MgO, Cement Concr. Res. 25 (1995) 51–56.
[15] L. Zheng, C. Xuehua, T. Mingshu, MgO-type delayed expansive cement, Cement Concr. Res. 21 (1991) 1049–1057.
[16] N. Marjanović, M. Komljenović, Z. Baščarević, V. Nikolić, R. Petrović, Physical–mechanical and microstructural properties of alkali-activated fly ash–blast furnace slag blends, Ceram. Int. 41 (2015) 1421–1435.
[17] M. Criado, A. Fernández-Jiménez, A. Palomo, Alkali activation of fly ash: effect of the SiO2/Na2O ratio: Part I: FTIR study, Microporous Mesoporous Mater. 106 (2007) 180–191.
[18] T. Omur, N. Miyan, N. Kabay, B. Birol, D. Oktay, Characterization of Ferrochrome Ash and Blast Furnace Slag Based Alkali-Activated Paste and Mortar, Constr Build Mater., 2022, 129805.
[19] N. Kabay, M. Mert, N. Miyan, T. Omur, Pumice as precursor in geopolymer paste and mortar, Journal of Civil Engineering and Construction 10 (2021) 225–236.
[20] B. Akturk, M. Abolfathi, S. Ulukaya, A.B. Kizilkanat, T.J.N. Hooper, L. Gu, E.-H. Yang, C. Unluer, Hydration kinetics and performance of sodium carbonate-activated slag-based systems containing reactive MgO and metakaolin under carbonation, Cem. Concr. Compos. (2022), 104617.
[21] A.F. Hashmi, M.S. Khan, M. Bilal, M. Shariq, A. Baqi, Green concrete: an eco-friendly alternative to the OPC concrete, Construction 2 (2022) 93–103.
[22] G.F. Huseien, K.W. Shah, Performance evaluation of alkali-activated mortars containing industrial wastes as surface repair materials, J. Build. Eng. 30 (2020), 101234.
[23] J. Kiventerä, P. Perumal, J. Yliniemi, M. Illikainen, Mine tailings as a raw material in alkali activation: a review, Int. J. Miner. Metall. Mater. 27 (2020) 1009–1020.
[24] H.M. Khater, M. Ghareib, Optimization of geopolymer mortar incorporating heavy metals in producing dense hybrid composites, J. Build. Eng. 32 (2020), 101684.
[25] M. Erdem, H.S. Altundoğan, M.D. Turan, F. Tümen, Hexavalent chromium removal by ferrochromium slag, J. Hazard Mater. 126 (2005) 176–182.
[26] N. Sahu, A. Biswas, G.U. Kapure, A short review on utilization of ferrochromium slag, Miner. Process. Extr. Metall. Rev. 37 (2016) 211–219.
[27] J. Zelić, Properties of concrete pavements prepared with ferrochromium slag as concrete aggregate, Cement Concr. Res. 35 (2005) 2340–2349.
[28] N.M. Kopuri, K. Ramesh, Durability studies on concrete with ferro chrome slag as partial replacement of fine aggregate, Int. J. Eng. Res. Technol. 8 (2019).
[29] C.R. Panda, K.K. Mishra, K.C. Panda, B.D. Nayak, B.B. Nayak, Environmental and technical assessment of ferrochrome slag as concrete aggregate material, Construct. Build. Mater. 49 (2013) 262–271.
[30] O. Gencel, F. Koksal, C. Ozel, W. Brostow, Combined effects of fly ash and waste ferrochromium on properties of concrete, Construct. Build. Mater. 29 (2012) 633–640.
[31] M.K. Dash, S.K. Patro, Effects of water cooled ferrochrome slag as fine aggregate on the properties of concrete, Construct. Build. Mater. 177 (2018) 457–466.
[32] B.B. Lind, A.-M. Fällman, L.B. Larsson, Environmental impact of ferrochrome slag in road construction, Waste Manag. 21 (2001) 255–264.
[33] M.B. Karakoç, I. Türkmen, M.M. Maraş, F. Kantarci, R. Demirboğa, M.U. Toprak, Mechanical properties and setting time of ferrochrome slag based geopolymer paste and mortar, Construct. Build. Mater. 72 (2014) 283–292.
[34] A. Özcan, M.B. Karakoç, The resistance of blast furnace slag-and ferrochrome slag-based geopolymer concrete against acid attack, Int. J. Civ. Eng. 17 (2019) 1571–1583.
[35] M. Elzeadani, D. V Bompa, A.Y. Elghazouli, One part alkali activated materials: a state-of-the-art review, J. Build. Eng. 57 (2022), 104871.
[36] I. Ismail, S.A. Bernal, J.L. Provis, S. Hamdan, J.S.J. van Deventer, Drying-induced changes in the structure of alkali-activated pastes, J. Mater. Sci. 48 (2013) 3566–3577, https://doi.org/10.1007/s10853-013-7152-9.
[37] M.A.H. Bhuyan, R.K. Gebre, M.A.J. Finnilä, M. Illikainen, T. Luukkonen, Preparation of filter by alkali activation of blast furnace slag and its application for dye removal, J. Environ. Chem. Eng. 10 (2022), 107051.
[38] F. Jorne, F.M.A. Henriques, L.G. Baltazar, Influence of superplasticizer, temperature, resting time and injection pressure on hydraulic lime grout injectability. Correlation analysis between fresh grout parameters and grout injectability, J. Build. Eng. 4 (2015) 140–151.
[39] F. Rosquoët, A. Alexis, A. Khelidj, A. Phelipot, Experimental study of cement grout: rheological behavior and sedimentation, Cement Concr. Res. 33 (2003) 713–722.
[40] A. Shahriar, M.L. Nehdi, Rheological properties of oil well cement slurries, Proceedings of the Institution of Civil Engineers-Construction Materials 165 (2012) 25–44.
[41] Y. Rifaai, A. Yahia, A. Mostafa, S. Aggoun, E.-H. Kadri, Rheology of fly ash-based geopolymer: effect of NaOH concentration, Construct. Build. Mater. 223 (2019) 583–594.
[42] K. Vance, A. Dakhane, G. Sant, N. Neithalath, Observations on the rheological response of alkali activated fly ash suspensions: the role of activator type and concentration, Rheol. Acta 53 (2014) 843–855.
[43] M.T. Tognonvi, D. Massiot, A. Lecomte, S. Rossignol, J.-P. Bonnet, Identification of solvated species present in concentrated and dilute sodium silicate solutions by combined 29Si NMR and SAXS studies, J. Colloid Interface Sci. 352 (2010) 309–315.
[44] J.F. Stebbins, I. Farnan, X. Xue, The structure and dynamics of alkali silicate liquids: a view from NMR spectroscopy, Chem. Geol. 96 (1992) 371–385.
[45] Y. Tardy, The chemistry of silica solubility, polymerization, colloid and surface properties, and biochemistry, Ralf K. Iler, 1979, Sciences Géologiques, Bulletins et Mémoires 35 (1982) 93.
[46] P. Wijnen, T.P.M. Beelen, J.W. De Haan, C.P.J. Rummens, L.J.M. Van de Ven, R.A. Van Santen, Silica gel dissolution in aqueous alkali metal hydroxides studied by 29Si NMR, J. Non-Cryst. Solids 109 (1989) 85–94.
[47] C. Lu, Z. Zhang, C. Shi, N. Li, D. Jiao, Q. Yuan, Rheology of alkali-activated materials: a review, Cem. Concr. Compos. 121 (2021), 104061.
[48] D.-W. Zhang, D. Wang, Z. Liu, F. Xie, Rheology, agglomerate structure, and particle shape of fresh geopolymer pastes with different NaOH activators content, Construct. Build. Mater. 187 (2018) 674–680.
[49] Q. Li, Y. Fan, S.P. Shah, Rheological properties and structural build-up of cement based materials with addition of nanoparticles: a review, Buildings 12 (2022) 2219.
[50] G. Fang, W.K. Ho, W. Tu, M. Zhang, Workability and mechanical properties of alkali-activated fly ash-slag concrete cured at ambient temperature, Construct. Build. Mater. 172 (2018) 476–487.

[51] X. Gao, Q.L. Yu, H.J.H. Brouwers, Reaction kinetics, gel character and strength of ambient temperature cured alkali activated slag–fly ash blends, Construct. Build. Mater. 80 (2015) 105–115.
[52] C.K. Yip, G.C. Lukey, J.L. Provis, J.S.J. van Deventer, Effect of calcium silicate sources on geopolymerisation, Cement Concr. Res. 38 (2008) 554–564.
[53] B. Chen, J. Wang, J. Zhao, Effect of sodium aluminate dosage as a solid alkaline activator on the properties of alkali-activated slag paste, Adv. Mater. Sci. Eng. (2021) 2021.
[54] A.A. Adam, N.H. Amiri, I.W. Suarnita, N. Rupang, The effect of lime addition on the setting time and strength of ambient cured fly ash based geopolymer binder, in: MATEC Web of Conferences, EDP Sciences, 2016, 01015.
[55] C.S. Thunuguntla, T.D.G. Rao, Effect of mix design parameters on mechanical and durability properties of alkali activated slag concrete, Construct. Build. Mater. 193 (2018) 173–188.
[56] A. Mehta, R. Siddique, T. Ozbakkaloglu, F.U.A. Shaikh, R. Belarbi, Fly ash and ground granulated blast furnace slag-based alkali-activated concrete: mechanical, transport and microstructural properties, Construct. Build. Mater. 257 (2020), 119548.
[57] I. Ismail, S.A. Bernal, J.L. Provis, R. San Nicolas, D.G. Brice, A.R. Kilcullen, S. Hamdan, J.S.J. van Deventer, Influence of fly ash on the water and chloride permeability of alkali-activated slag mortars and concretes, Construct. Build. Mater. 48 (2013) 1187–1201.
[58] P. Nath, P.K. Sarker, Effect of GGBFS on setting, workability and early strength properties of fly ash geopolymer concrete cured in ambient condition, Construct. Build. Mater. 66 (2014) 163–171.
[59] T. Phoo-Ngernkham, V. Sata, S. Hanjitsuwan, C. Ridtirud, S. Hatanaka, P. Chindaprasirt, High calcium fly ash geopolymer mortar containing Portland cement for use as repair material, Construct. Build. Mater. 98 (2015) 482–488.
[60] K. Chen, W.-T. Lin, Q. Liu, B. Chen, V.W.Y. Tam, Micro-characterizations and geopolymerization mechanism of ternary cementless composite with reactive ultra-fine fly ash, red mud and recycled powder, Construct. Build. Mater. 343 (2022), 128091.
[61] D.B. Kumarappa, S. Peethamparan, Quantification of drying shrinkage in alkali activated slag mortars and validating the efficiency of various shrinkage mitigation methods, Transp. Res. Board TRB. (2017) 1–13.
[62] B. Lothenbach, A. Gruskovnjak, Hydration of alkali-activated slag: thermodynamic modelling, Adv. Cement Res. 19 (2007) 81–92.